geosciences

MDPI

Article

Comparison of Geometric and Volumetric Methods to a 3D Solid Model for Measurement of Gully Erosion and Sediment Yield

Ingrid Luffman [1,*], Arpita Nandi [1] and Benjamin Luffman [2]

[1] Department of Geosciences, East Tennessee State University, Johnson City, TN 37614, USA; nandi@etsu.edu
[2] Department of Mechanical, Aerospace and Biomedical Engineering, The University of Tennessee, Knoxville, TN 37996, USA; bluffman@vols.utk.edu
* Correspondence: luffman@etsu.edu; Tel.: +1-423-439-7551

Received: 30 January 2018; Accepted: 28 February 2018; Published: 3 March 2018

Abstract: Gully erosion is a global problem that degrades land and reduces its utility for agriculture, development, and water quality. Quantification of sediment yield and control of sediment sources is essential for environmental protection. Five methods to evaluate erosion rates and sediment yield on an east Tennessee, USA, hillslope were compared: (1) physical measurement by removal of accumulated sediment using 10 L buckets; (2) repeated measurement of erosion pins in gully (erosional) and delta (depositional) areas; (3) geometric model using a combination trapezoidal prism-cylinder segment; (4) geometric model using a series of trapezoidal pyramids; and (5) 3D solid computer modeling. The 3D solid model created in SolidWorks was selected as the reference model and all other methods overestimated sediment yield to varying degrees. Erosion pin methods overestimated sediment yield by 368% in deltas and 123% in gullies. Volumetric measurement of sediment using buckets overestimated sediment yield by 160% due to void space in the buckets. The trapezoidal prism-cylinder segment model overestimated sediment yield by 66% and the trapezoidal pyramids method overestimated sediment yield by 5.7%. For estimation of sediment trapped behind an elliptical or circular silt fence dam, use of the trapezoidal pyramid method provides a good approximation comparable to 3D solid computer modeling.

Keywords: sediment yield; gully erosion; sediment volume; silt fence; 3D solid model

1. Introduction

Gully erosion is a global problem that degrades land and reduces its utility for agriculture, development, and water quality. Gully erosion begins with overland flow that concentrates into rivulets and erodes small rills. Over time rills erode into gullies which are a significant cause of land degradation and soil loss worldwide [1,2]. Eroded sediment from gullies is a primary sediment source, increasing nutrient loadings in runoff that impacts water quality downstream [2]. Given the persistent environmental effects of gully erosion, and its contribution to water quality impairments, quantification of sediment yield and control of sediment sources is essential to protect water quality [3].

In a comprehensive review of gully erosion research [4], gully erosion research sites were classified by climate; ~40% of gully erosion research was found to be conducted in humid climates (Koppen-Geiger precipitation classification "fully humid" (f)). Interestingly, only 11.5% of research was conducted in arid climates, with the remaining 26.7% conducted in seasonally wet/dry climates. Sites were also classified by land use (grazing—40.5%, agriculture—43.2%, forest—13.2%, and urban—3.1%) and lithology (sedimentary, at 67.7%, was the most common). Over 30% of the studies measured degradation rates at various time scales from short to long term, while other studies assessed

factors and processes responsible for erosion (23.1%) and developed models to quantify or predict erosion (16.9%).

Gully erosion is complex, and gully initiation and development results from many different causes, under different climates, at different spatial and temporal scales [4]. Significant climatic and physical drivers for gully erosion are precipitation [5,6], freeze-thaw activity [7–11], wind [12,13], and gravity-driven mass wasting [14].

South-Eastern USA has been identified as a hot spot for widespread gully erosion, and the region's humid climate and predominantly sedimentary geology make it a good representative region for gully erosion research. Average erosion rates on the Appalachian Piedmont have been measured to range from 0.04 mm/year to 2.47 mm/year [15–19]. In Tennessee's Ridge and Valley physiographic province, erosion in a badlands-type gully system vary with geomorphic setting: 43 mm/year on interfluves, 5.9 mm/year on sidewalls, and 11.6 mm/year in channels, measured over a two year period [11]. These measurements were made using erosion pins installed in multiple transects throughout the gully system. Interestingly, erosion (pin lengthening) and deposition (pin shortening) in gully channels tended to cancel each other out, suggesting that significant sediment may be stored in the gullies themselves.

Several gully erosion sediment yield estimation methods are reported in the literature. Accepted methods to estimate gully erosion include erosion pins [20–23], geometric estimates of material eroded or deposited [24–26], feature based assessments [20], and volumetric measures of material deposited or trapped by physical capture of sediment in sediment trap buckets [27,28], or by modeling pre- and post-depositional surfaces [29].

The use of erosion pins to measure gully erosion is well established [20–23]. Pins are installed in the soil and exposed length is measured. Over time erosion increases the length of the pins and deposition decreases it. Periodic repeated measures of pin length captures erosion and depositional events at each pin. Frequent measurement is desired so that a high temporal resolution dataset may be obtained and erosion associated with single storm events may be quantified.

Measurement of gully features, including scour holes and headcut locations have also been used to quantify gully erosion. For example, 34 gully features were monitored in Australia's seasonally wet-dry climate for headward advance or retreat, enlargement, or infilling [20]. Erosional features with depths of 0.2–1.5 m and widths of 0.3–8 m changed little over the five year study period, and hillslope-channel coupling was identified, suggesting that sediment has residence time on the hillslope and in the gullies. The authors concluded that despite the lack of change during the study period, the gullies were at a tipping point for rapid headward movement and expansion.

Two reviews of geometric sediment estimation methods for sediment trapped behind check dams for various channel geometries were published recently [3,30]. The Prism method [24] is employed when the channel is V-shaped and the volume of accumulated sediment (VP) is modeled with a trapezoidal prism using $VP = \frac{1}{4} \times l_s \times h \times (w_b + w_s)$, where l_s = length of sediment wedge perpendicular to check dam, h = height of sediment wedge from base of dam, w_b is the width of the channel downstream of the check dam, and w_s is the mean width of the sediment wedge. Other models for various wedge tapers in both length and width were also presented [30].

The Pyramid method [25] is employed in trapezoidal channels, and models the volume of accumulated sediment (V) using a horizontal pyramid with a trapezoidal base such that $V = 1/3 \times b \times h$ where b = area of trapezoid base in contact with check dam and h = length of sediment wedge. Other Pyramid methods for different wedge tapers were also presented [30].

Rectangular models have a rectangular area in contact with the check dam, but taper upstream height-wise and also possibly width-wise [30]. In that study, the authors propose criteria to select an appropriate model, based on field measurements of the check dam and channel.

The Trapezoids method assumes a U-shaped streambed, and divides the sediment wedge into sections. The volume of each section is calculated using the most appropriate geometric shape for the section cross-section, and the sections are summed to obtain the total wedge volume [3,31].

Furthermore, the Sections method models the wedge by dividing it into slices for which the volume is estimated and summed to obtain the total volume of the wedge. Sediment weight is determined from the total volume and the bulk density of the wedge sediment [26].

Of the geometric methods, the Prism [24] and Pyramid [25] methods tend to underestimate sediment retained by check dams by 21% and 16%, respectively [26], and 24.5% and 29.3%, respectively [3] when compared to the Sections method, which is deemed the most representative. Furthermore, the Trapezoids method overestimates trapped sediment volume by 24.8% [3].

The digital terrain model geospatial method measures the wedge volume by modeling the original stream channel using other nearby unsilted channels to develop a 3D digital surface for the channel base. A 3D wedge surface is then developed from a high resolution topographic dataset obtained in the field. Subtraction of the two surfaces using a GIS leaves the 3D wedge, for which volume and weight (using bulk density) may be calculated [3,29]. This digital geospatial method produces variable results (both overestimation and underestimation). Two other digital methods have also been used for gully delineation. A GIS based normalized topographic method using digital elevation model (DEM) data was employed across a wide range of scales from rills to badlands, with higher accuracy in gully volume calculations in smaller gully systems [32]. A low-cost and rapid tool to monitor gully erosion using overlapped images taken from a handheld camera along a predefined walking path, then assembled using a structure from motion (SfM) algorithm, was compared to results obtained using a terrestrial laser scanner system [33]. While the terrestrial laser scanner underestimated the gully volume due to shadowing effects, SfM provided views of the gully interior that helped eliminate shadows and increased accuracy in sediment yield calculations. SfM has also been employed to monitor erosion associated with single events at high temporal resolution (15 s intervals), capturing short term processes and geomorphic change with sub-cm accuracy [34]; and for efficiently reconstructing a 3D gully from a series of cross-sections created from smartphone camera images processed using the free tool FreeXSapp [35].

Monitoring of stream stage and turbidity can be used to calculate sediment yield by first establishing the stream rating curve for discharge, and modeling the correlation between turbidity and Suspended Sediment Concentration (SSC) for both rising and falling discharge. Sediment yield is estimated by integrating the product of discharge and SSC over time [36].

Noteworthy developments in producing prototypes using 3D models for 3D printing offer the ability to dynamically display, analyze, and interpret field data [37]. Among geoscientists, paleontologists were the first group to adopt this technology [38–40]. With the availability of high-quality, high-resolution datasets on Earth's structure and surface, the geoscientific community has begun to embrace 3D model printing technology in work involving geomorphology, stratigraphy, terrestrial topography, and seismic studies [41–44]. While computer-aided 3D solid models have yielded realistic replicas of the real-world, no prior studies have applied this technique to sediment transport, deposition, or yield. The most closely related study investigated 3D printed river cobbles in relation to weathering processes [45].

In the absence of check dams, silt fences may be employed as an economical method to estimate soil erosion on hillslopes [46], and may have certain advantages over check dams for small catchments. For example, check dams allow passage of finer particles (silt and clay) through the gabion walls, and have a trap efficiency of as low as 35% [47], but potentially as high as 97.7% [3]. Silt fences, in comparison, have small openings (0.3–0.8 mm) and a high tensile strength (0.3–0.4 kN), and are therefore useful for temporary detention and storage of sediment [46]. Silt fence trap efficiency for a field study on a fallow agricultural plot with silt loam soil ranged from 73% to 100%, with a seasonal average of 93% [48].

While sediment yield estimation methods behind check dams are widespread in the literature, no studies have looked into sediment yield estimation behind curved silt fences, which generally produces an elliptical shaped delta area, very different from the ones produced behind straight-faced check dams. Additionally, application of 3D solid computer models in sediment yield estimation

can provide a new dimension which is not explored in current studies. To bridge the knowledge gap, the objective of this present study is to compare different volumetric and geometric sediment yield estimation methods in an elliptical fan shaped gully depositional area with a realistic 3D solid computer generated model.

2. Materials and Methods

2.1. Study Area and Field Setup

This study was performed on an eroding hillslope in the Ridge and Valley physiographic province, east Tennessee, USA (36°25′20.1″ N, 82°32′39.1″ W). Soils are clay-rich ultisols (Collegedale-Etowah complex, CeD3), categorized as Acrisols, according to the World Reference Base for Soil. These soils have an erodibility factor of 0.28 indicating susceptibility to rill and gully erosion [49]. The typical soil profile in the study area consisted of a thin surface O-horizon, followed by a fine grained sand and silt layer, grading into silty clay [50]. The climate is Humid Subtropical (Köppen-Geiger classification Cfa) with hot summers, mild winters, and year-round precipitation [51]. Average annual rainfall is 1040 mm with average temperature ranging from 1.1 °C in winter to 23.3 °C in summer. The property was previously used for cattle pasture, and the gullies have developed over a period of nearly 30 years, based on analysis of historical air photos [50]. Gully depths and widths range from 0.5 m to 2.5 m and 3.5 m to 5.5 m, respectively, and the annual erosion rate for the complete 3870 m^2 (0.387 ha) gully system was calculated from erosion pin data in 2013 at 30 mm/year, with a sediment yield of 116.26 m^3/year [6].

A single gully within the system was selected for this study with an area of 544 m^2 (0.0544 ha) measured with ArcGIS 10.3 (ESRI, Redlands, CA, USA). Gully cross-sections are V-shaped upstream and trapezoidal downstream closer to the delta area. A silt fence (0.9 m high by 11.53 m long) was installed in the delta area to capture sediment eroded from the gully. Twelve 5 mm diameter steel erosion pins were installed in the delta area to measure deposition behind the silt fence, and 13 erosion pins were installed in three transects throughout the gully (Figure 1). Transects were selected on mature portions of the gully that were physically representative of the gully.

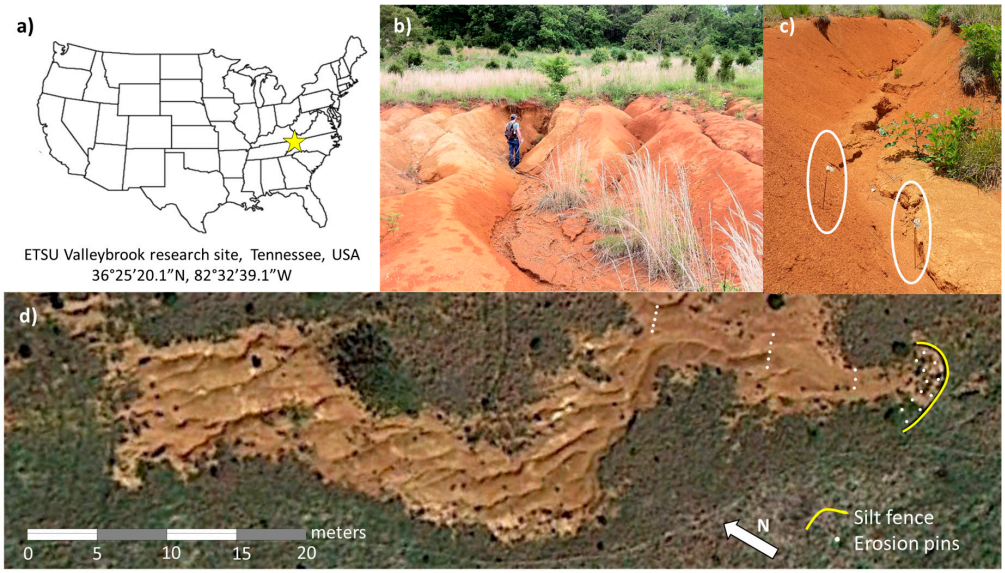

Figure 1. Gully system location and setting (modified after Luffman et al. (2015)). (**a**) Geographic location of study area; (**b**) a typical gully in the system; (**c**) erosion pins (circled) are 0.5–1 m long, with exposed length approximately 30 cm in this image; (**d**) aerial view of the studied gully, silt fence is outlined in yellow and pins in delta and gully area are marked with white circles. Aerial image from Google Earth (2012 imagery).

2.2. Erosion Estimation Methods

2.2.1. Bucket Method

Sediment accumulation behind the silt fence was measured for three time-periods: 16 February 2011 to 11 May 2012 (456 days); 18 May 2012 to 17 August 2012 (94 days); and 21 August 2012 to 27 February 2013 (192 days). At the end of each time period, accumulated sediment was removed manually from the depositional area (delta) using shovels and 10 liter buckets. The number of buckets was recorded and the extracted sediment was deposited down gradient and therefore removed from the system. The original vegetation and soil O horizon were used as a marker horizon for the initial time period. For subsequent periods, red chalk was distributed over the delta area to form a marker horizon for a lower bound of sediment deposition immediately after sediment removal for the prior period. Sediment volume was totaled and adjusted for lost sediment using a trap efficiency ratio of 93% [48]. Erosion rate in m^3/year (m^3/y) was calculated.

2.2.2. Erosion Pins

Erosion pin lengths were measured on 25 April 2011, 11 May 2012, and approximately weekly thereafter following established methods [6]. Three time periods were used, as closely matching the time periods for the bucket method as possible: 25 April 2011 to 11 May 2012 (382 days); 23 May 2012 to 17 August 2012 (85 days); and 29 August 2012 to 23 February 2013 (178 days). Positive change indicated deposition during the measurement period, while negative change indicated erosion (Figure 2).

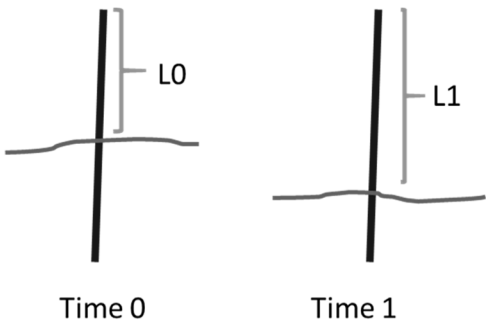

Figure 2. Erosion results in increased exposed length of erosion pins at Time 1 (L1), such that change in exposed length (L0–L1) is negative for erosion and positive for deposition.

The volume of sediment deposited in the delta area (Figure 3a) was estimated by multiplying the average change in delta pin length by the surface area of the delta, and then scaling for an assumed trap efficiency of 93%. The surface area of the delta was modeled using a sector of an ellipse by extracting the silt fence outline from an aerial image, fitting an ellipse to obtain semi-major (a) and semi-minor (b) axes (Figure 3b). Arc length was calculated using Farooque's method [52] and goodness of fit of the ellipse was assessed by comparison of the calculated arc length for the fitted ellipse with the measured arc length of the silt fence (w, Figure 3b).

The angle (θ) between sides x and y (Figure 3c) was calculated using the law of cosines

$$x^2 = y^2 + z^2 - 2yz \times cos\theta \quad (1)$$

where x and y are the distances between vertex A and the ends of the silt fence, while z is the length of the chord connecting the ends of the silt fence, all measured in the field using a tape measure.

Surface area was calculated using [53]

$$F(\varphi) = \frac{ab}{2}\left[\varphi - \tan^{-1}\left(\frac{(b-a)\sin 2\varphi}{(b+a)+(b-a)\cos 2\varphi}\right)\right] \quad (2)$$

where φ is the angle measured from the semi major axis to the sector edge. Because the delta area intersected two quadrants of the ellipse (Figure 3b), total area was calculated from the sum of the area of the lower right quadrant $F(90°)$ and the area of the upper right quadrant $F(\varphi)$.

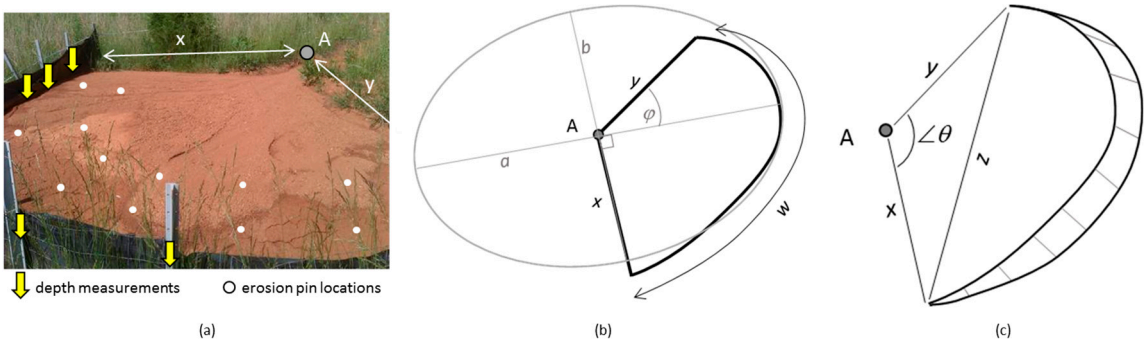

Figure 3. Delta area (**a**) was approximated by delineating the depositional zone, fitting an ellipse to the silt fence boundary, and summing the area of the delta sectors overlapping the lower and upper right quadrants of the ellipse (**b**). Wedge angle θ was calculated using the law of cosines (**c**).

For gully pins, the change in pin length for the n = 13 pins installed in the three transects uphill of the delta was averaged. Erosion rate in m^3/y was estimated using the gully area (544 m^2) which was calculated using ArcGIS 10.3 (ESRI, Redlands, CA, USA).

2.2.3. Geometric Methods

The sediment wedge accumulated behind the silt fence can be visualized as pie-shaped, with pie thickness diminishing to zero at all three vertices (Figure 3c). Unlike sediment wedges that accumulate behind gabion basket check dams, the silt fence dam was elliptical and therefore assuming a flat downstream face for the sediment wedge would not be correct. This complicated the channel geometry, and none of the geometric methods developed or evaluated by Ramos-Diez et al. (2016; 2017) [3,30] were deemed appropriate for this site without modification. Therefore, the sediment wedge volume was calculated using two different combinations of geometric shapes: a trapezoidal prism-cylinder segment combination (Figure 4a) and a series of adjacent trapezoidal pyramids (Figure 4b).

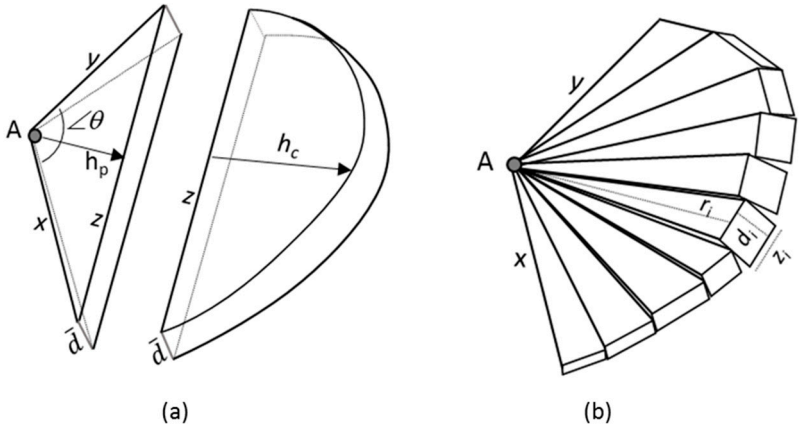

Figure 4. Geometric approximation of sediment wedge volume: (**a**) using a trapezoidal prism and cylinder segment; (**b**) using a series of adjacent trapezoidal pyramids.

The surface geometry of the wedge of accumulated material in the delta was measured. The sediment wedge depth was recorded at i = 11 fence posts along the arc, beginning and ending at areas of zero accumulation at the end posts. Depth was measured from the original ground surface on

the downstream side of the silt fence, to the current sediment surface on the upstream side. Mean depth between each pair of posts (d_i) was calculated and averaged to obtain a single number representing depth $\overline{d}$ of sediment accumulation along the arc. The distance from point A to each post and the distance between posts (z_i) was recorded.

First, the wedge volume was approximated by the sum of the areas of a trapezoidal prism and a cylinder segment (Figure 4a). The volume of the trapezoidal prism (V_P) was calculated using

$$V_P = \frac{1}{3}\,\overline{d} * z * h_p \tag{3}$$

where $\overline{d}$ is the average thickness of the wedge at the silt fence, z is the length of the chord connecting the fence edges, and h_p is the height of triangle XYZ calculated from its area using Heron's formula [54]

$$Area\ \Delta XYZ = \sqrt{p(p-x)(p-y)(p-z)} \tag{4}$$

$$p = \frac{(x+y+z)}{2} \tag{5}$$

And x and y are previously defined as the distances from A to each end of the silt fence. The volume of the cylinder segment (V_c) was calculated using [55]

$$V_C = \overline{d}\left[R^2 \cos^{-1}\left(\frac{R-h_c}{h_c}\right) - (R-h_c)\sqrt{2Rh_c - {h_c}^2}\right] \tag{6}$$

$$R = \frac{(x+y)}{2} \tag{7}$$

$$h = R\left(1 - \cos\frac{\theta}{2}\right) \tag{8}$$

And the volume of the sediment wedge was therefore the sum $V = Vp + Vc$.

Second, the wedge volume was approximated by a series of trapezoidal pyramids, similar to the pyramid method [25], but modified to a sum of adjacent trapezoidal pyramid volumes (V_i) assembled in a fan shape (Figure 4b) using the sum of the volumes of i trapezoidal prisms (Equation (3))

$$V = \sum_{i=1}^{10} V_i = \frac{1}{3}\sum_{i=1}^{10} r_i d_i z_i \tag{9}$$

where r_i is the average distance between A and posts i and $i + 1$, d_i is the average of sediment depth at posts i and $i + 1$, and z_i is the distance between posts i and $i + 1$. Sediment yield was adjusted to account for a 93% trap efficiency for both geometric estimation methods.

2.2.4. The 3D Solid Model

The sediment wedge was modeled using the 3D solid modeling program SolidWorks 2016 [56], using dimensions measured in the field: distance from vertex A to each fencepost (r'_i), distance between fence posts (z_i), and depth of sediment at each fencepost (d'_i) (Figure 5). This method differs from the trapezoidal pyramid method in that the base of each pyramid was modeled as an irregular polygon. The model was drawn by first creating a sketch of the base of the sediment wedge (Figure 3). Each section of the wedge was extruded to the measured depth, and a 3-D sketch was used to define the upper surface of the section relative to the adjacent section and vertex A. Each section was trimmed to the correct size using a cut extrude defined by the 3-D sketch. Sediment yield was calculated in m^3/y and adjusted to account for a 93% trap efficiency.

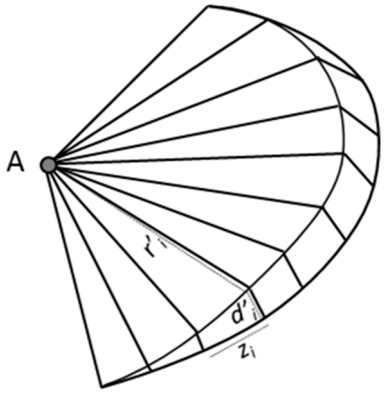

Figure 5. Input geometry for the 3D computer model of the sediment wedge.

3. Results

3.1. Bucket Method

Sediment accumulation behind the silt fence dam during the three periods was variable, ranging from 8.92 m^3/y to 33.44 m^3/y, with an average of 14.43 m^3/y, after adjusting for trap efficiency (Table 1).

Table 1. Sediment accumulation behind silt fence dam, volume measured by sediment removal using 10 L buckets.

Date	Days	Buckets (10 L)	Volume (m^3)	Deposition Rate (m^3/y)	Scaled for 93% Trap Efficiency (m^3/y)
16 February 2011 to 11 May 2012	456	1036	10.36	8.29	8.92
18 May 2012 to 17 August 2012	94	801	8.01	31.10	33.44
21 August 2012 to 27 February 2013	192	891	8.91	16.94	18.21
Totals or averages	742	2728	27.28	13.42	14.43

3.2. Erosion Pins

The semi major and semi minor axes of the fitted ellipse were a = 6.544 m and b = 4.475 m, respectively. The sector angle (θ) was 124.2° and therefore the depositional zone surface area was calculated as 34.45 m^2, a sum of the two elliptical sectors of areas 11.45 m^2 (φ = 34.2°) and 23.0 m^2 (φ = 90°). The modeled arc length of 12.56 m overestimated the measured length of 11.53 m by 9.0%.

Erosion rate from the gully and deposition of the eroded sediment in the delta area were averaged for three periods (Table 2). Erosion rate in the gully was 22.7 mm/year with a sediment yield of 12.3 m^3/y, calculated using the measured gully area of 544 m^2. The deposition rate in the delta was 699.9 mm/year, with a sediment accumulation rate of 25.9 m^3/y. During the first period (25 April 2011 to 11 May 2012), the gully experienced net deposition (positive sediment yield of 20.1 m^3/y), and during the second period (23 May 2012 to 16 August 2012) that sediment was transported out of the gully into the delta area where a sharp increase in sediment accumulation was recorded (42.7 m^3/y).

3.3. Geometric Methods

The trapezoidal prism–cylinder segment method produced an estimated sediment wedge volume of 10.53 m^3, and a sediment yield of 9.19 m^3/y after scaling for a 93% trap efficiency. The trapezoidal pyramid method produced an estimated sediment wedge volume of 6.71 m^3, with a sediment yield of 5.85 m^3/y after accounting for trap efficiency (Table 3).

Table 2. Erosion pin change in length for delta pins (n = 12) and gully pins (n = 13). Positive values denote deposition and negative values denote erosion.

Dates	Days	Gully			Delta			
		Average Pin Change (mm)	Erosion (–) Rate (mm/year)	Sediment Yield (m^3/y)	Average Pin Change (mm)	Deposition (+) Rate (mm/year)	Sediment Accummlation (m^3/y)	Accummlation Adjusted for 93% Trap Efficiency (m^3/y)
25 April 2011 to 11 May 2012	382	38.6	36.9	20.1	207.8	198.6	6.8	7.4
23 May 2012 to 16 August 2012	85	−10.7	−45.9	−25.0	288.9	1240.6	42.7	46.0
29 August 2012 to 23 February 2013	178	−28.8	−59.0	−32.1	322.1	660.5	22.8	24.5
Average		−0.3	−22.7	−12.3	272.9	699.9	24.1	25.9

Table 3. Sediment wedge volume calculation for trapezoidal pyramid method.

Trapezoidal Segment i	Average Depth (m) d_i	Width (m) z_i	Average Radius (m) r_i	Volume (m^3) V_i
1	0.08	1.19	4.49	0.14
2	0.22	1.30	4.41	0.42
3	0.29	1.04	4.47	0.45
4	0.39	1.25	4.81	0.78
5	0.45	1.30	5.36	1.04
6	0.42	1.17	5.69	0.92
7	0.44	0.84	5.78	0.70
8	0.45	0.81	5.79	0.70
9	0.46	1.02	5.73	0.88
10	0.24	1.63	5.22	0.68
Total Volume				6.71
Sediment yield (m^3/y)				5.45
Scale for 93% trap efficiency (m^3/y)				5.85

3.4. 3D Computer Model

The 3D solid model of the sediment wedge had a volume of 5.69 m^3 and a surface area of 27.9 m^2, 19% less than the area modeled using a fitted ellipse (Figure 6).

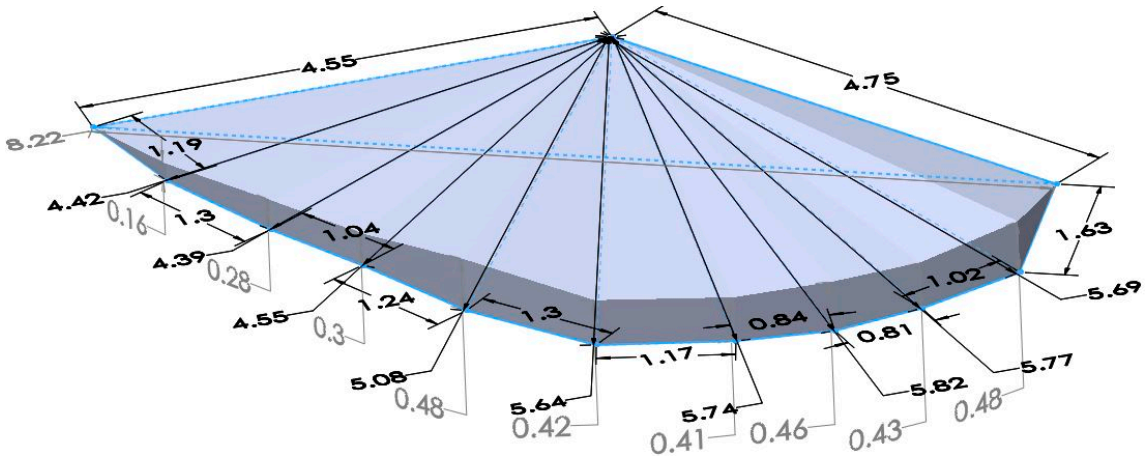

Figure 6. 3D solid model created in SolidWorks 2016.

4. Discussion

This study provided a comparative, quantitative analysis of sediment yield measurement in an elliptical delta setting, using five different methods including buckets, erosion pins, two geometric models, and a 3D solid model.

The bucket method was the most direct way of calculating sediment deposition in the gully delta area that estimated 14.43 m^3/y sediment yield (Table 4). This approach, however, had the highest possibility of human induced error from bucket under- or overloading during sediment removal. Additionally the 'cut and fill' effect generated additional volume due to air space created during bucket loading.

The erosion pin method, another accepted method in the literature, provided quantitative estimates of sediment erosion in the gully and sediment deposition in the downgradient delta area. Ideally erosion should balance deposition after accounting for silt fence trap efficiency, however in the present study, using erosion pins, the sediment deposited in the delta was almost double the sediment eroded from the gully (Table 4). The erosion pins were installed in three transects in a small, mature portion of the gully that physically represented the entire gully system. Additionally, erosion pins in

the delta were located in the area of greatest deposition to capture the maximum sediment loading. However, the results from this study suggest that monitoring erosion and deposition using additional transects throughout the gully systems, rather than targeting areas of highest erosion and deposition, has the potential to produce a more realistic outcome. During the first study period (25 April 2011 to 11 May 2012), sediment eroded from the gully area was redeposited in the gully farther downstream, and was not transported to the delta until the second study period (Table 2). In the second and third study periods the opposite pattern was documented. The sediment load balance between eroding and depositing areas may have varied due to the varying lengths of the intervals and their timing relative to seasonal fluctuating weather patterns including summer precipitation and winter freeze thaw effects [11].

Table 4. Comparison of results.

Method		Sediment Yield (m^3/y)	% Yield Difference	Considerations
Buckets		14.43	160	Air space in buckets, overfilling. Inability to remove all sediment in one day, additional deposition during removal may cause overestimation.
Erosion Pins	Gully	12.33	123	Pins represent small part of eroding area. Eroded sediment may be redeposited in gully.
	Delta	25.93	368	Delta pins located in area of greatest deposition and no pins installed on shallow margins of sediment wedge.
Geometric	Trapezoidal prism/cylinder segment	9.19	66	Depth was averaged across wedge face. Depth at fence assumed to equal depth along chord z. Elliptical silt fence approximated with cylinder. Base and surface of wedge assumed to be planar.
	Sum of trapezoidal pyramids	5.85	5.7	Fence assumed to be planar between fence posts, with negligible bowing between posts. Base and surface of wedge assumed to be planar.
3D model		5.54	-	Fades from measurable depth to zero depth in end segments. Continuous sediment surface and base.

The two geometric methods (trapezoidal prism–cylinder segment and trapezoidal pyramids) yielded slightly different results. In both geometric models, the base and top of sediment wedge were assumed to be planar while in reality the surfaces were slightly uneven, a surface that could not be measured in the present study. Specifically, the trapezoidal prism–cylinder segment model assumed the average depth across the wedge face (chord *z* in Figure 4a) was equal to the average depth at the silt fence, a value used in the both the trapezoidal prism and in the cylinder segment volume calculations, which resulted in an overestimation of sediment volume of 66% for the trapezoidal prism–cylinder segment model. Furthermore, the trapezoidal pyramid model assumed a planar face of the silt fence between each pair of fence posts, with a discontinuous sediment wedge surface. In reality the silt fence bulged slightly from the sediment load behind the fence and the sediment wedge surface was neither stepped between each segment (Figure 4b) nor completely planar. Both contributed to errors in the true volume estimation and resulted in a marginal overestimation (5.7%) of sediment yield in the gully delta.

When evaluating effectiveness of methods to predict sediment yield in an elliptical shaped depositional area, the 3D solid model created in SolidWorks was selected as the reference model. For the model, all input dimensional data: distance from wedge vertex A (center of the ellipse) to each fencepost, distance between fence posts, and depth of sediment at each fencepost, were collected in the field, and the sediment surface and base of each pyramid were entered as continuous, irregular polygons that taper to zero depth at end segments. Therefore, the output from the 3D solid model most realistically represented the actual gully depositional volume.

The trapezoidal pyramids geometric model was closest to the 3D solid model, as the majority of the model measurements were also made in the field, and average sediment depth ranged from zero to

maximum to account for shallow and deep margins of the sediment wedge throughout the deposition area. The slight overestimation of this model (5.7%) from the 3D solid model can be explained by the way the base of each pyramid was modeled—as series of discontinuous rectangles whose widths were calculated as average sediment depth between two consecutive fence posts, contrary to the continuous, irregular polygons used in the 3D model. The trapezoidal prism—cylinder segment model was the second closest approximation, which produced a representative scenario, with the exception that the model could not handle the change in deposition depth from the silt fence to the chord z in Figure 4a. In the present study, the erosion pin method produced 123% and 368% overestimation of erosion in the gully and delta areas, respectively. In future, the erosion pins method can estimate results more accurately, provided erosion pins are installed uniformly and extensively throughout the eroding area, to represent different parts of the gully system. The bucket method, while easy to implement, was unable to account for under- and overfilling of the buckets caused by voids or mounding that occurred while loading the buckets. This produced a 160% overestimation of the sediment yield.

Comparison with other studies indicates that all but one of the methods compared in this study significantly overestimated sediment volume compared to several other studies. For example, the Prism [24] and Pyramid [25] geometric methods underestimated sediment retained by check dams from 16% to 29% [3,26], while our trapezoidal prism/cylinder segment model overestimated by 66%. The Trapezoids method of summing perpendicular sections transverse to the gully length [3] overestimated sediment volume by ~25%.

These other studies were performed on larger dams, with heights ranging from 1.3 m to 4.1 m, widths from 5.5 m to 13.2 m, and wedge lengths from 4.9 m to 55.7 m [3]. Our depositional area was comparable only to the smallest of these, with a height of 0.9 m, arc length of 11.5 m, and wedge length ranging from 4.4 m to 5.8 m. Comparison of our errors to the smallest checkdams, revealed similar direction of error (overestimation), and our errors were comparable in size for our trapezoidal prisms method (overestimation of 5.7%, Table 4).

5. Conclusions

This study compares geometric, volumetric, and 3D solid modeling methods to evaluate erosion rates and sediment yield for a sediment wedge trapped behind a silt fence dam. Two new geometric methods are presented (trapezoidal prism-cylinder segment and trapezoidal pyramids). All methods overestimate sediment yield compared to the reference method (3D solid model), however the trapezoidal prism method had the smallest error, overestimating sediment yield by 5.7%, which is comparable to overestimation measured in similar sized gullies using other geometric methods.

The availability of 3D printing software technology for 3D solid modeling presents numerous possibilities to investigate geomorphological process. The present study is the first of its own kind to adapt 3D printing software as a practical tool to estimate sediment yield in gully delta system. To improve the general applicability of the studied models including 3D solid models, future research should be performed in multiple elliptical gullies with varied delta sizes. Overall, in the absence of 3D modeling software, the new trapezoidal pyramid model presented in this study can produce a reasonable estimate of sediment volume trapped in elliptical shaped delta areas.

Acknowledgments: The authors gratefully acknowledge the assistance of undergraduate research assistants Tim Spiegel, Trevor Wilson, and Nicolas Barnes for assistance with sediment removal and Daniel Firth for valuable feedback in development of the geometric volumetric methods. The authors also gratefully acknowledge financial support from the Department of Geosciences, East Tennessee State University for funds to purchase field equipment and supplies and for support from East Tennessee State University Honors College for two student-faculty collaborative research grants.

Author Contributions: Arpita Nandi and Ingrid Luffman conceived and designed the experiments and completed the field data collection. Ingrid Luffman analyzed the data; Benjamin Luffman developed the 3D solid model; Ingrid Luffman and Arpita Nandi wrote the paper.

Conflicts of Interest: The authors declare no conflict of interest.

References

1. Poesen, J.; Nachtergaele, J.; Verstraeten, G.; Valentin, C. Gully erosion and environmental change: Importance and research needs. *Catena* **2003**, *50*, 91–133. [CrossRef]
2. Valentin, C.; Poesen, J.; Yong, L. Gully erosion: Impacts, factors and control. *Catena* **2005**, *63*, 132–153. [CrossRef]
3. Ramos-Diez, I.; Navarro-Hevia, J.; San Martin Fernandez, R.; Diaz-Gutierrez, V.; Mongil-Manso, J. Evaluating methods to quantify sediment volumes trapped behind check dams, Saldana badlands (Spain). *Int. J. Sediment Res.* **2017**, *32*, 1–11. [CrossRef]
4. Castillo, C.; Gómez, J.A. A century of gully erosion research: Urgency, complexity and study approaches. *Earth Sci. Rev.* **2016**, *160*, 300–319. [CrossRef]
5. Nearing, M.A.; Jetten, V.; Baffaut, C.; Cerdan, O.; Couturier, A.; Hernandez, M.; Le Bissonnais, Y.; Nichols, M.H.; Nunes, J.P.; Renschler, C.S. Modeling response of soil erosion and runoff to changes in precipitation and cover. *Catena* **2005**, *61*, 131–154. [CrossRef]
6. Luffman, I.E.; Nandi, A.; Spiegel, T. Gully morphology, hillslope erosion, and precipitation characteristics in the Appalachian Valley and Ridge province, southeastern USA. *Catena* **2015**, *133*, 221–232. [CrossRef]
7. Gatto, L.W.; Ferrick, M.G. *Overland Erosion due to Freeze—Thaw Cycling Cold Regions Research Overland Erosion Due To Freeze—Thaw Cycling*; Cold Regions Research and Engineering Laboratory: Hanover, NH, USA, 2003.
8. Ferrick, M.G.; Gatto, L.W. Quantifying the effect of a freeze-thaw cycle on soil erosion: Laboratory experiments. *Earth Surf. Process. Landf.* **2005**, *30*, 1305–1326. [CrossRef]
9. Zhang, J.; Liu, S.; Yang, S. The classification and assessment of freeze-thaw erosion in Tibet. *J. Geogr. Sci.* **2007**, *17*, 165–174. [CrossRef]
10. Kong, B.; Yu, H. Estimation model of soil freeze-thaw erosion in Silingco watershed wetland of northern Tibet. *Sci. World J.* **2013**, *2013*, 1–7. [CrossRef] [PubMed]
11. Barnes, N.; Luffman, I.; Nandi, A. Gully erosion and freeze-thaw processes in clay-rich soils, northeast Tennessee, USA. *GeoResJ* **2016**, *9*, 67–76. [CrossRef]
12. Yan, F.L.; Shi, Z.H.; Li, Z.X.; Cai, C.F. Estimating interrill soil erosion from aggregate stability of Ultisols in subtropical China. *Soil Tillage Res.* **2008**, *100*, 34–41. [CrossRef]
13. Marzen, M.; Iserloh, T.; de Lima, J.L.M.P.; Ries, J.B. The effect of rain, wind-driven rain and wind on particle transport under controlled laboratory conditions. *Catena* **2016**, *145*, 47–55. [CrossRef]
14. Guerra, A.J.T.; Fullen, M.A.; Jorge, M.D.C.O.; Bezerra, J.F.R.; Shokr, M.S. Slope processes, mass movement and soil erosion: A review. *Pedosphere* **2017**, *27*, 27–41. [CrossRef]
15. Reusser, L.; Bierman, P.; Rood, D. Quantifying human impacts on rates of erosion and sediment transport at a landscape scale. *Geology* **2015**, *43*, 171–174. [CrossRef]
16. Cain, S.A. Pollen Analysis of Some Buried Soils, Spartanburg County, South Carolina. *Bull. Torrey Bot. Club* **1944**, *71*, 11–22. [CrossRef]
17. Hack, J.T. *Rock Control and Tectonism—Their Importance in Shaping the Appalachian Highlands*; U.S. Geological Survey: Reston, VA, USA, 1978.
18. Staheli, A.C.; Ogren, D.E.; Whorton, C.H. Age of swamps in the Alcovy River drainage basin. *Southeast. Geol.* **1974**, *16*, 102–106.
19. Matthews, W.H. Cenozoic erosion and erosion surfaces of eastern North America. *Am. J. Sci.* **1975**, *275*, 818–824. [CrossRef]
20. Hancock, G.R.; Evans, K.G. Gully, channel and hillslope erosion—An assessment for a traditionally managed catchment. *Earth Surf. Process. Landf.* **2010**, *35*, 1468–1479. [CrossRef]
21. Hudson, N. *Field Measurement of Soil Erosion and Runoff*; Food & Agriculture Organization: Rome, Italy, 1993; Volume 68, ISBN 9251034060.
22. Keay-Bright, J.; Boardman, J. Evidence from field-based studies of rates of soil erosion on degraded land in the central Karoo, South Africa. *Geomorphology* **2009**, *103*, 455–465. [CrossRef]
23. Smith, H.G.; Dragovich, D. Sediment budget analysis of slope–channel coupling and in-channel sediment storage in an upland catchment, southeastern Australia. *Geomorphology* **2008**, *101*, 643–654. [CrossRef]
24. Castillo, V.M.; Mosch, W.M.; García, C.C.; Barberá, G.G.; Cano, J.A.N.; López-Bermúdez, F. Effectiveness and geomorphological impacts of check dams for soil erosion control in a semiarid Mediterranean catchment: El Carcavo (Murcia, Spain). *Catena* **2007**, *70*, 416–427. [CrossRef]

25. Romero-Díaz, A.; Alonso-Sarriá, F.; Martínez-Lloris, M. Erosion rates obtained from check-dam sedimentation (SE Spain). A multi-method comparison. *Catena* **2007**, *71*, 172–178. [CrossRef]
26. Díaz, V.; Mongil, J.; Navarro, J. Topographical surveying for improved assessment of sediment retention in check dams applied to a Mediterranean badlands restoration site (Central Spain). *J. Soils Sediments* **2014**, *14*, 2045–2056. [CrossRef]
27. Ashida, K.; Takahashi, T.; Sawada, T. Sediment Yield and Transport on a Mountainous Small Watershed. *Bull. Disaster. Prev. Res. Inst.* **1976**, *26*, 119–144.
28. Namikas, S.L. Field Evaluation of Two Traps for High-Resolution Aeolian Transport Measurements. *J. Coast. Res.* **2002**, *18*, 136–148. [CrossRef]
29. Sougnez, N.; van Wesemael, B.; Vanacker, V. Low erosion rates measured for steep, sparsely vegetated catchments in southeast Spain. *Catena* **2011**, *84*, 1–11. [CrossRef]
30. Ramos-Diez, I.; Navarro-Hevia, J.; Fernández, R.S.M.; Díaz-Gutiérrez, V.; Mongil-Manso, J. Geometric models for measuring sediment wedge volume in retention check dams. *Water Environ. J.* **2016**, *30*, 119–127. [CrossRef]
31. Bellin, N.; Vanacker, V.; van Wesemael, B.; Solé-Benet, A.; Bakker, M.M. Natural and anthropogenic controls on soil erosion in the internal betic Cordillera (Southeast Spain). *Catena* **2011**, *87*, 190–200. [CrossRef]
32. Castillo, C.; Taguas, E.V.; Zarco-Tejada, P.; James, M.R.; Gómez, J.A. The normalized topographic method: An automated procedure for gully mapping using GIS. *Earth Surf. Process. Landf.* **2014**, *39*, 2002–2015.
33. Kaiser, A.; Neugirg, F.; Rock, G.; Müller, C.; Haas, F.; Ries, J.; Schmidt, J. Small-Scale Surface Reconstruction and Volume Calculation of Soil Erosion in Complex Moroccan Gully Morphology Using Structure from Motion. *Remote Sens.* **2014**, *6*, 7050–7080. [CrossRef]
34. Eltner, A.; Kaiser, A.; Abellan, A.; Schindewolf, M. Time lapse structure-from-motion photogrammetry for continuous geomorphic monitoring. *Earth Surf. Process. Landf.* **2017**, *42*, 2240–2253. [CrossRef]
35. Castillo, C.; Marín-Moreno, V.J.; Pérez, R.; Muñoz-Salinas, R.; Taguas, E.V. Accurate automated assessment of gully cross-section geometry using the photogrammetric interface FreeXSapp. *Earth Surf. Process. Landf.* **2018**. [CrossRef]
36. Didoné, E.J.; Minella, J.P.G.; Merten, G.H. Quantifying soil erosion and sediment yield in a catchment in southern Brazil and implications for land conservation. *J. Soils Sediments* **2015**, *15*, 2334–2346. [CrossRef]
37. De Paor, D.G. Virtual Rocks. *GSA Today* **2016**, *26*, 4–22. [CrossRef]
38. Bristowe, A.; Parrott, A.; Hack, J.; Pencharz, M.; Raath, M. A non-destructive investigation of the skull of the small theropod dinosaur, Ceolophysis rhodesiensis, using CT scans and rapid prototyping. *Palaeontol. Afr.* **2004**, *40*, 31–36.
39. Hasiotis, S.T.; Hirmas, D.R.; Platt, B.F.; Raynolds, J. New frontiers in ichnology using MLT (Multistripe Laser Triangulation) and rapid prototyping technology for three-dimensional analysis, printing, and sharing of modern and ancient traces with other ichnophiles. In *Northeastern (46th Annual) and North-Central (45th Annual) Joint Meeting of the Geological Society of America Abstracts with Programs*; Geological Society of America: Pittsburgh, PA, USA, 2011; p. 81.
40. Hyatt, J.A.; Rosiene, J. Preparing image maps, physical models, and analyzing topographic form using terrestrial laser scanning data collected at Dinosaur State Park, Rocky Hill, CT. In Proceedings of the Northeastern Section Geological Society of America 48th Annual Meeting; Geological Society of America: Bretton Woods, NH, USA, 2013; pp. 53–56.
41. Horowitz, S.S.; Schultz, P.H. Printing space: Using 3D printing of digital terrain models in geosciences education and research. *J. Geosci. Educ.* **2014**, *62*, 138–145. [CrossRef]
42. Hasiuk, F.J.; Harding, C. Touchable topography: 3D printing elevation data and structural models to overcome the issue of scale. *Geol. Today* **2016**, *32*, 16–20. [CrossRef]
43. Hasiuk, F.J.; Harding, C.; Renner, A.R.; Winer, E. TouchTerrain: A simple web-tool for creating 3D-printable topographic models. *Comput. Geosci.* **2017**, *109*, 25–31. [CrossRef]
44. Hasiuk, F. Making things geological: 3-D printing in the geosciences. *GSA Today* **2014**, *24*, 28–29. [CrossRef]
45. Bourke, M.; Viles, H.; Nicoli, J.; Lyew-Ayee, P.; Ghent, R.; Holmund, J. Innovative applications of laser scanning and rapid prototype printing to rock breakdown experiments. *Earth Surf. Process. Landf.* **2008**, *33*, 1614–1621. [CrossRef]

46. Robichaud, P.R.; Brown, R.E. *Silt Fences: An Economical Technique for Measuring Hillslope Soil Erosion*; US Department of Agriculture, Forest Service, Rocky Mountain Research Station: Washington, DC, USA, 2002.
47. Martín-Rosales, W.; Pulido-Bosch, A.; Gisbert, J.; Vallejos, A. Sediment yield estimation and check dams in a semiarid area (Sierra de Gádor, southern Spain). *IAHS-AISH Publ.* **2003**, 51–58.
48. Robichaud, P.R.; McCool, D.K.; Pannkuk, C.D.; Brown, R.E.; Mutch, P.W. Trap Efficiency of Silt Fences Used in Hillslope Erosion Studies. In Proceedings of the International Symposium on Soil Erosion for the 21st Century, Honolulu, HI, USA, 3–5 January 2001; pp. 541–543. [CrossRef]
49. United States Department of Agriculture. *Washington County Soil Survey Report*; United States Department of Agriculture: Washington, DC, USA, 2011.
50. Nandi, A.; Luffman, I. Erosion related changes to physicochemical properties of Ultisols distributed on calcareous sedimentary rocks. *J. Sustain. Dev.* **2012**, *5*, 52–68. [CrossRef]
51. Kottek, M.; Grieser, J.; Beck, C.; Rudolf, B.; Rubel, F. World map of the Köppen-Geiger climate classification updated. *Meteorol. Zeitschrift* **2006**, *15*, 259–263. [CrossRef]
52. Khan, M.F. Arc length of an elliptical curve. *Int. J. Sci. Res. Publ.* **2013**, *3*, 1–5.
53. Eberly, D. The Area of Intersecting Ellipses. Available online: https://www.geometrictools.com/Documentation/AreaIntersectingEllipses.pdf (accessed on 10 January 2018).
54. Weisstein, E.W. Heron's Formula. Available online: http://mathworld.wolfram.com/HeronsFormula.html (accessed on 20 January 2018).
55. Weisstein, E.W. Horizontal Cylindrical Segment. Available online: http://mathworld.wolfram.com/HorizontalCylindricalSegment.html (accessed on 10 January 2018).
56. Dassault Systemes SA SolidWorks 2016. Available online: https://www.3ds.com/products-services/solidworks/ (accessed on 10 January 2018).